

R. GRAF^{1,*}
A. FERNANDEZ^{1,*}
M. DUBOV²
H.J. BRUECKNER³
B.N. CHICHKOV⁴
A. APOLONSKI^{5,6,✉}

Pearl-chain waveguides written at megahertz repetition rate

¹ Max Planck Institute of Quantum Optics, Hans-Kopfermann-Str. 1, 85748 Garching, Germany
² Photonics Research Group, Aston University, Birmingham B4 7ET, UK
³ Fachhochschule Oldenburg/Ostfriesland/Wilhelmshaven, University of Applied Sciences, Constantiaplatz 4, 26723 Emden, Germany
⁴ Laser Zentrum Hannover e.V., Hollerithallee 8, 30419 Hannover, Germany
⁵ Ludwig-Maximilians-Universität München, 85748 Garching, Germany
⁶ Institute of Automation and Electrometry, SB RAS, Novosibirsk 630090, Russia

Received: 22 August 2006/

Revised version: 11 September 2006

Published online: 9 November 2006 • © Springer-Verlag 2006

ABSTRACT Waveguides in the form of connected pearls, written with sub-30 fs pulses centered at 800 nm at a repetition rate of 10 MHz, show high changes of the refractive index and, as a consequence, simple in-coupling. The value of the refractive index modification of these waveguides is as high as 10^{-2} , optical losses are 6 dB/cm (at 1.55 μm) and the mode field diameter is 8 μm at 670 nm.

PACS 42.62.-b; 87.80.Mj; 42.82.Et

1 Introduction

Femtosecond (fs) light pulses can successfully modify transparent material on a μm and even nm scale [1–3]. Among different structures, waveguides are of great interest for realizing all-optical chips, sensors, etc. They are a basic component of μm -scale devices written in bulk media. The waveguides can be written with light sources of two types: laser systems at a kHz repetition rate (oscillator + amplifier) and laser oscillators at a repetition rate of 1–100 MHz. The difference between these two approaches lies in the accumulated thermal effects. In the case of MHz repetition rates, the residual heat effects from a previous light pulse are present for the next pulses, modifying the pulse interaction with the medium [4–7]. Usually, thermal effects lead to production of smoother and broader transversal structures than those obtained in the absence of these effects. Additionally, MHz repetition rates provide the further important advantage of high-speed material modification. This allows writing of high-quality structures due to the stable pulse energy and good beam pointing stability. The difference in the speed of waveguide fabrication between these two approaches can be as high as three orders of magnitude. Thermal effects also

help to produce waveguides with larger diameter, thus decreasing their losses and increasing the coupling efficiency. Experiments show that the waveguide losses decrease as the repetition rate of the writing laser increases [7, 8].

The lowest losses demonstrated in fused silica with MHz repetition rate so far are ~ 1 dB/cm in waveguides written at a speed of 15 mm/s [7, 8]. The pulse energies hitherto used in this regime range from 5 nJ to 5 μJ . In a recent publication [9] waveguides with losses ~ 0.2 dB/cm were demonstrated. They were written at kHz repetition rate. All waveguides fabricated and investigated so far look like smooth structureless objects, except for one experiment [9], where complex waveguide structures were formed by single pulses (losses > 1 dB/cm).

This paper reports the fabrication and investigation of a novel type of waveguide, written at a repetition rate of 10 MHz with a high energy – up to 40 nJ, sub-30 fs pulses. These waveguides look like a chain of connected pearls and can be written at a high speed with an optimum at 1 mm/s. They have several interesting features that can be useful for photonics and for the production of micro-channels with modulated diameter. Traditional smooth waveguides were also written at the lower pulse energies – below 26 nJ.

2 Experimental and characterization techniques

The experimental setup is shown in Fig. 1. The light source is a sub-30 fs 10 MHz 200 nJ Ti:Sa oscillator [10]. An external compressor readily allowed pre-chirping of the pulses such that they are the shortest on the target. We monitored the pulse duration with an auto-correlator and by introducing the equal amount of glass right in front of the auto-correlator we were able to pre-compensate any pulse broadening due to the thickness of the focusing objective. The stability of the pulse train was controlled with a fast photodetector and oscilloscope. The spectrum generated and the relevant autocorrelation trace are shown in Fig. 2. An aspheric lens (Thorlabs, $f = 4.5$ mm, $\text{NA} = 0.55$) was used for focusing radiation into the sample. To estimate the pulse distortion due to chromatic aberration we made the same experiments with an achromatic objective ($f = 6$ mm, $\text{NA} = 0.2$) and received

✉ Fax: +49 (0) 89 289 14141,
E-mail: apolonSKI@physik.uni-muenchen.de

*Contributed equally.

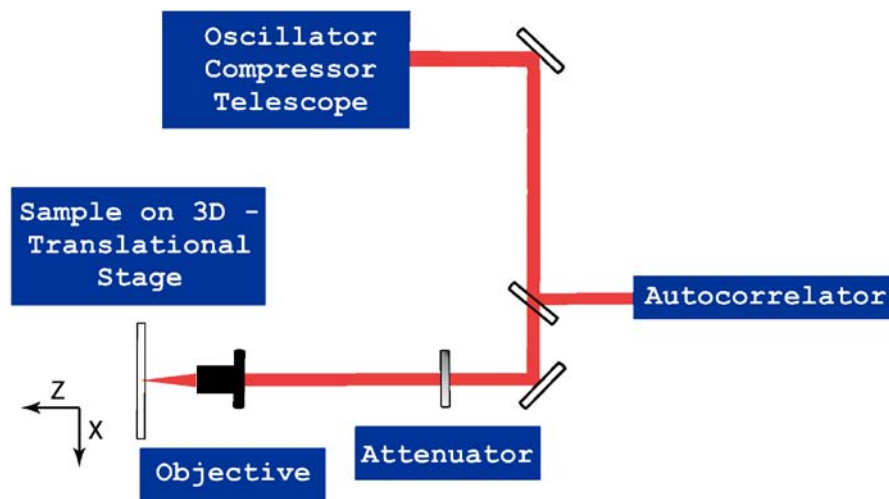


FIGURE 1 Experimental setup

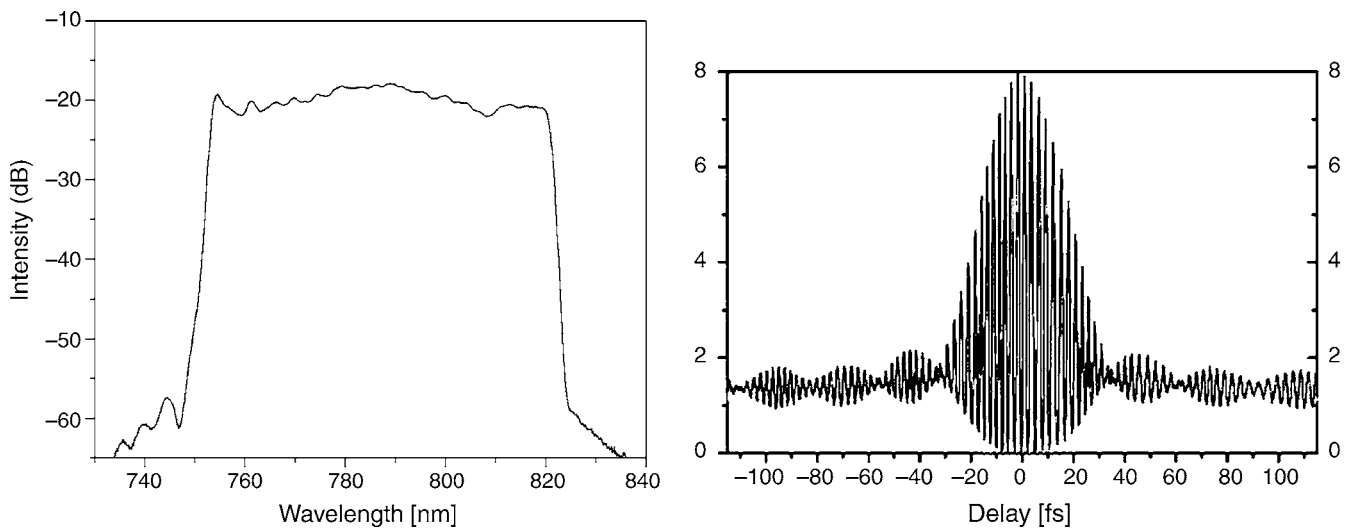


FIGURE 2 Generated spectrum (left) – note vertical dB scale, and corresponding interferometric autocorrelation trace (right)

similar structures and the same dependence on the pulse energy. A telescope provided optimization of the beam diameter (4 mm) at the objective. The beam waist was monitored with a beam profiler with the micro-objective; its value was below $2 \mu\text{m}$ at the level of $1/e^2$. A variable neutral attenuator enabled the pulse energy on the sample surface to be adjusted with a precision of 0.1 nJ. The sample was a high-quality $25 \times 50 \times 1$ mm fused silica plate (Saint Gobain Quartz) or BK7 glass sample. The written structures in these two materials were almost identical, except for the necessary pulse energy, which was less in the case of BK7. Below, we present results only for fused silica samples. The sample was fixed to a computer-controlled 3D-translational stage (PI, model 505.1PD) with the maximum writing speed of 50 mm/s and a resolution of 250 nm. The sample was fixed vertically and translated in the horizontal direction. The beam polarization was also in the horizontal plane. All the structures were written inside the sample, 0.1–0.3 mm beneath the surface. Special precautions had been made to minimize the pulse energy deviations and beam pointing fluctuations. The positioning accuracy was measured on the basis of experiments with the fabrication of crossing structures in the sample and was found to be of the order of $1 \mu\text{m}$. The maximum writing deviations from

a straight line at a distance of 10 mm were measured from the experimental data and are equal to $1 \mu\text{m}$.

After writing the structures, the samples were cut and polished. The mode of the outgoing radiation was measured at two wavelengths: 670 nm and 1559 nm. Coupling into the waveguides was provided through fiber SM 3224; in the case of 1559 nm it was SMF-28. For coupling, diode lasers (by Thorlabs) were used and the output was measured with a micro-objective and a CCD camera.

The value of the refractive index modification in the fabricated waveguides was characterized by measuring their mode field diameter at different wavelengths with further reconstruction. The spatial variations of the refractive index were retrieved by the phase retardation technique. It is known that the phase variations of a coherent laser field can be recovered from intensity measurements in the adjacent planes with the help of the transport-of-intensity equation [11, 12]. This method is proved to be applicable for the phase retardation measurements in objects on the micrometer scale with the refractive index contrast as low as 10^{-4} when light microscopy is used. Another advantage of this technique is that the phase map over the whole field of view of the microscope can be retrieved from the same measurement. However, reconstruction

of the 3D profile of the refractive index distribution requires additional information – the depth of the phase object along the integration axis (Z axis in our case). For the phase measurements, we used the commercial QPM software (IATIA, www.iatia.com.au) and an optical microscope equipped with a CCD camera and a sample stage movable in the Z direction (Axioscope 2M, Zeiss).

3 Results

Figure 3 shows the evolution of waveguide structures as a function of the pulse energy under otherwise fixed conditions. At a pulse energy of approximately 20 nJ, a smooth line-like structure readily becomes visible in the optical microscope, corresponding to traditional waveguides. At higher energies starting from 27 nJ (low-energy threshold), the appearance of a new pearl-chain structure is observed. Physically, this structure represents waveguides with quasi-periodically modulated diameter. Writing at energies higher than 27 nJ is accompanied by visible white light generation with a characteristic spectrum as shown in Fig. 4.

3.1 Smooth “standard” waveguides; multiple scans

Smooth waveguides appeared only at laser energies below 26 nJ. The transversal cross-section is elongated in the direction of light propagation and is equal to $(2-3) \times$

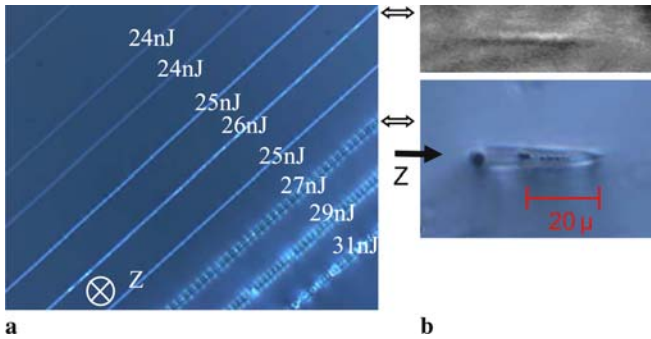


FIGURE 3 Waveguide structures written in the fused silica sample, 200 μm beneath the surface, at different pulse energies (shown for each scan) and a constant speed of 0.25 mm/s. *Right:* transversal structures corresponding to smooth (*top*) and pearl-chain (*below*) waveguides. The complex structure in the *lower inlet* incorporates several small (above the *red scale bar*) and (nearest to the incident writing laser) one biggest, round micro-void-like material modifications. The direction (Z) of the incident light is shown by the *black arrow*

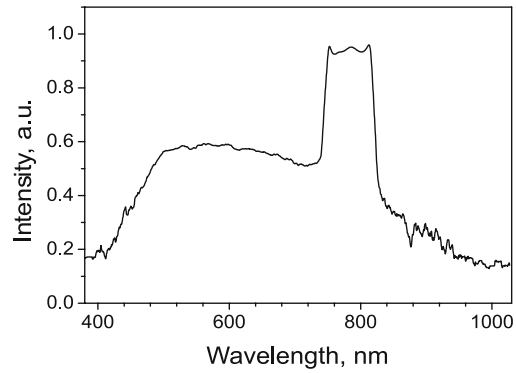


FIGURE 4 White light spectrum generated in the sample at pulse energies higher than 27 nJ. The laser spectrum around 800 nm is also shown

40 μm , see upper inlet in Fig. 3. The modification of the refractive index can be enhanced by multiple scanning over the same waveguide, as shown in Fig. 5. Coupling into a waveguide of this type was found to be possible but very difficult because of its strongly elliptic cross-section. Micro-objectives with higher NA can help to fabricate round waveguide structures of this type, as was already demonstrated in experiments with astigmatic beams [5].

3.2 Pearl-chain waveguides; structure and transmission

A very sharp transition from smooth structures to pearl-chains was observed at a pulse energy of 26 nJ as shown in Fig. 3. During the index measurement routine, we found that the pearl might have a complex structure as one could see from a set of microscopic Z -scan images presented in Fig. 6. The images of the cross-section of the pearl presented on the bottom inlet in Fig. 3 revealed a rather complicated structure, similar to what was reported earlier in [13]. The dynamics of the creation of such a micro-void-like structure is not completely clear yet. We will discuss it briefly below.

Above this low-energy threshold the formation of pearls happens at all writing speeds, provided that the laser pulses are chirp-free. The pearl-chain structure exhibits high index modification and shows good guiding properties. The structure becomes irregular at pulse energies above 29 nJ (high-energy threshold) and light guiding through such high-energy-written pearl structures is weak, mainly due to scattering. Just above the low-energy threshold, the separation between the

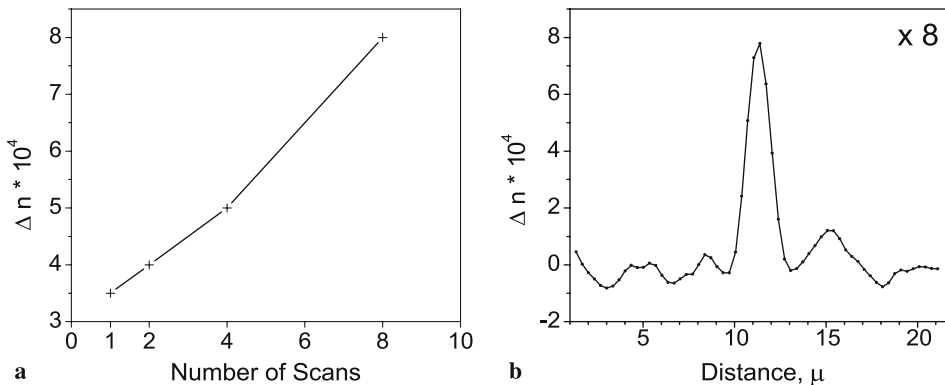


FIGURE 5 Change in the refractive index contrast vs. the number of consecutive scans (*left*), and the cross section of the refractive index in a smooth waveguide for the case of eight consecutive scans (*right*)

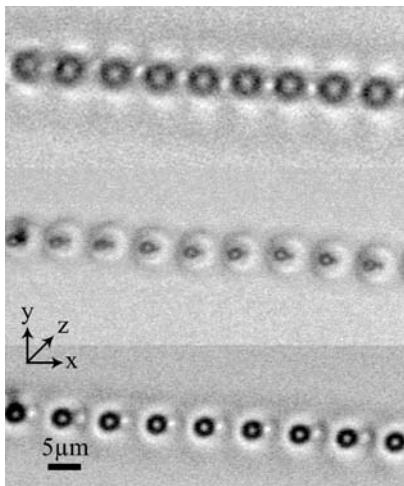


FIGURE 6 Pearl-chain structure under a light microscope. Microscopic top view at different focusing positions into the structure (depth variations). The writing light comes from the top

pearls is large, but the spacing is filled up with pearls with increasing number of scans. For pulse energies well above the low-energy threshold but below the high-energy threshold, one scan is enough to produce quasi-periodically connected pearls similar to those in Fig. 6. Below the low-energy threshold, pearls can only be produced by illuminating one spot for several seconds without moving the sample. This allows arbitrary structures to be produced using pearls as building elements.

The pearl structure is shown in Fig. 6 at different adjustments of the microscope objective into the sample. One can see an internal sharp structure of the pearl. Another feature of the written structure is its high periodicity ($\pm 5\%$). The distance between the pearls is a weak function of the writing speed, which was varied between 0.25 mm/s to 50 mm/s. We observed that only at speeds higher than 5 mm/s does the structure period become longer and we found that the highest regularity and also the highest guiding efficiency is achieved at a writing speed of 1 mm/s. The transversal pearl view shown in Fig. 3 (lower inlet) demonstrates rather a complex structure, consisting of the main waveguide, a second round component with a smaller diameter and 6–7 small round components separated by 1 μm . It is noteworthy that the main waveguide is perfectly round in contrast to the elongated transversal structure of smooth waveguides. A modified area around the pearl can be seen after phase reconstruction and has a size of 15 μm . The variation of the refractive index within the pearl for the near-the-threshold inscription intensity is shown in Fig. 7. The accumulated value (in the z -direction, see Fig. 6) of the refractive index modification in the central peak is as high as 1×10^{-2} on the assumption that the structure length is known. The shape of the refractive index structure depends on the writing pulse energy and could form a narrow gap instead of a peak at higher pulse energies.

In addition to the structures shown in Fig. 3, the structures of two crossing lines of this waveguide type were written and are shown in Fig. 8. One can see that in the range of overlap there are alternating sub-ranges with and without visible double structure. It looks like the top pearl blocks the creation

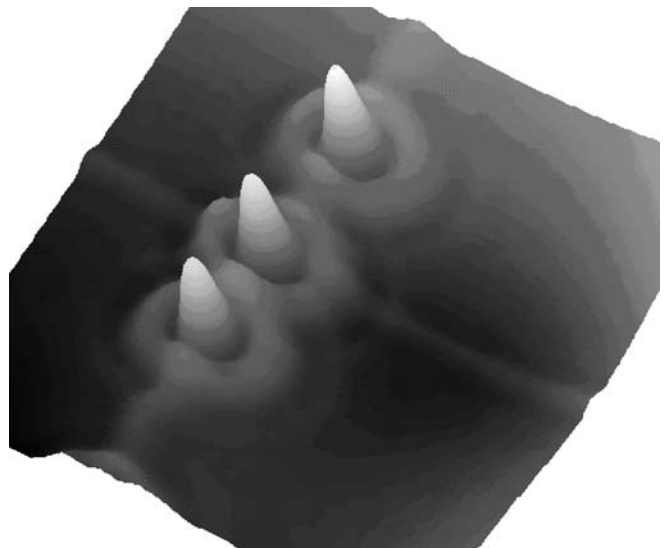


FIGURE 7 Accumulated phase retardation of the pearls, measured at a wavelength of 450 nm. The material becomes more optically dense in the center of the pearl and at its border. The intensity of the laser corresponds to the threshold for pearl formation. There is a visible cross with the previously formed smooth waveguide at the position of the middle pearl



FIGURE 8 X-coupler written with crossing pearl-chain waveguides

of a new one at the same place, or the threshold is higher for a second run. Such first X-couplers demonstrated a promising 80 : 20 division ratio without any optimization at all. At a wavelength of 670 nm the pearl-chain structures guided in a single- or multi-mode regime depending on the coupling beam adjustment, see Fig. 9. We are not completely sure if the weaker upper part in Fig. 9b is due to guiding in the second waveguide, consisting of smaller pearls (see the lower inlet of Fig. 3) via coupling from one waveguide to the other or a higher mode was excited. At a wavelength of 1559 nm only single-mode guiding is observed, see Fig. 10. In this case SMF-28 fiber was used to couple light in, and a different cam-

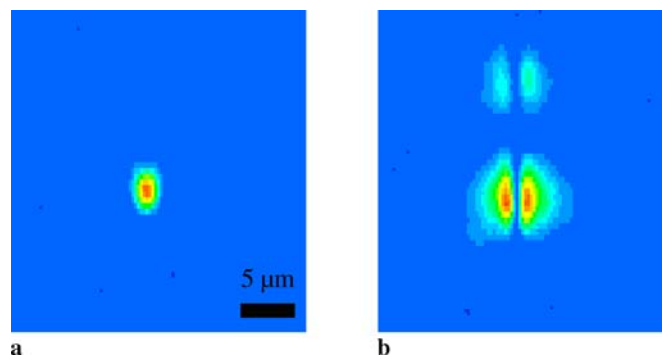


FIGURE 9 Two modes of the pearl-chain waveguide at a wavelength of 670 nm, depending on the beam adjustment: fundamental (left) and high-order (right)

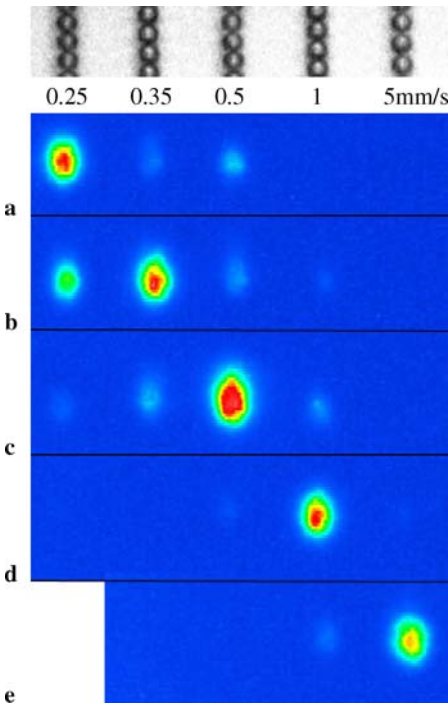


FIGURE 10 Guidance through 5 parallel pearl-chains at a wavelength of 1559 nm. The waveguides are separated by $18\ \mu\text{m}$ and written at different speeds (shown above the mode pictures). *Top*: waveguide view from top. One can see slightly different distances between pearls at a writing speed of 5 mm/s. Because of the small separation of the individual waveguides we observed faint coupling to the neighbouring structures as well

era, more sensitive in the infrared. The radiation was then coupled into a certain waveguide in an array of five parallel pearl-chain waveguides as shown in Fig. 10, one by one (Fig. 10a–e). One can see that coupling into one waveguide is accompanied by radiation transfer into the neighboring waveguides because of the small distance between them ($18\ \mu\text{m}$). All these waveguides were written at the same energy (44 nJ, but not chirp-free pulses) using different speeds. Coupling into the first waveguide is accompanied by coupling to two other waveguides; coupling into the second one results in partial coupling into the first, third and fourth waveguides. The waveguide written at 1 mm/s exhibits the strongest guiding strength. We did not observe any crosstalk between the waveguides, when the separation was bigger than $25\ \mu\text{m}$. The measured attenuation is 6 dB/cm.

3.3 White light generation during pearl-chain waveguide writing

We observed that the intensity of white light generation increases with the writing speed, other parameters being kept fixed. The white light disappears when the writing beam is stopped. After the first scan, performed at the maximum writing speed, the separation between pearls in the structure is large. After the second scan over this structure, the white light intensity becomes less and new pearls appear in the gap between the initial pearls. After several scans (10 at 50 mm/s and 4 scans at 5 mm/s), a dense pearl structure similar to that shown in Fig. 3 (written at 27 nJ) is observed, which is accompanied by very weak white light generation.

3.4 Mode-field diameter simulation

The eccentricity of the near-field intensity distribution is 10.9 : 8.0 at 1559 nm (Fig. 10). We simulated the waveguide performance with a circular gradient profile of the refractive index as shown in Fig. 7. The only parameter to vary was the peak refractive index contrast. The best fit of experimental data obtained at 1559 nm was achieved with an index contrast of $\Delta n = 0.019$. The optimal fit was further verified at a wavelength of 670 nm, where reasonably good agreement with the experiment was also established. Thus, the simulated mode field diameter was $8.2\ \mu\text{m}$, whereas the experimentally measured value was $8\ \mu\text{m}$. The eccentricity of the intensity distribution is about 5.7:3.1 at 670 nm.

4 Discussion and comparisons

4.1 Refractive index contrast of smooth waveguides

For multiple scans, a decrease of the refractive index contrast (for longitudinal writing geometry) with the number of scans was found in [14]. In our experiments on transverse inscription, the refractive index contrast grows almost linearly with the number of scans for operation below the low-energy threshold for pearls appearing, provided that the modified length is known. This can be a powerful way of optimizing smooth waveguides, provided that the writing accuracy is high enough. Our experience revealed that there are some limits to this index contrast enhancement, since after a number of scans one can have spontaneous pearls forming on a top of a smooth track. Transversally elongated structures, in the direction of light propagation, similar to those shown in Fig. 3, have been realized in several experiments [1, 5] with low-NA ($\text{NA} < 0.7$) micro-objectives. In our case the elongation of the smooth structure in the direction of the beam is slightly bigger than might be expected.

4.2 Pearl-chain waveguide modes

The modes shown in Figs. 9 and 10 correspond to LP_{01} and LP_{11} , if the fiber terminology can be applied in this case. In fibers, the number of guided modes is determined by the V parameter:

$$V = \frac{2\pi}{\lambda} a \sqrt{(n_1^2 - n_0^2)},$$

where a is a “core radius” ($2\ \mu\text{m}$ in our case), $\lambda = 0.8\ \mu\text{m}$, $n_0 = 1.45$.

For the LP_{11} mode, V must be > 3.6 . This means that according to the equation above, the change of refractive index is $> 10^{-2}$, which is in a good agreement with the independent measurements based on the phase retardation technique shown in Sect. 2, and obtained as a result of fitting in Sect. 3.4. A high refractive index change leads to a high numerical aperture NA of the waveguide, which is equal to $\text{NA} = \sqrt{2n_0\Delta n}$. In our case, for $\Delta n = 0.01$ we obtain $\text{NA} \approx 0.18$, more than for a single mode fiber.

4.3 White light spectrum

In our experiments, the threshold peak power for the white light generation was 1.7 MW. From the literature it is known that white light generation usually accompanies

a collapse of an optical pulse due to the nonlinear self-focusing effect [15–17]. The threshold power for the last process is not less than P_{cr} , and often it is higher than critical power [16]. In fused silica $P_{\text{cr}} = 2.3$ MW, if we take $n_2 = 2.5 \times 10^{-16}$ cm²/W, where n_2 is the nonlinear refractive index of fused silica. Thus, in our experiments white light generation occurs at a power *lower* than P_{cr} . What was also noticeable is that the white light intensity was weaker at lower writing speed, so white light generation takes place only during material “modification”. After it was modified, no further light generation takes place at all. This is perhaps, due to perturbations to the focused beam by areas with previously modified refractive index or when the void-like structures were formed.

Another possible reason for a broad light spectrum observed (see Fig. 4) is a black-body thermal radiation. If so, the temperature is about 5000 K in accordance with Planck’s law. This is just estimation, since the fit did not match the measured spectrum well, probably due to the uncalibrated detector at the edges of the spectral range or absence of thermal equilibrium. The temperatures of this level could give rise to a set of new physical effects, commonly referred in relation with the fiber fuse [18–22].

4.4 Possible mechanisms for pearl-chain structures

At lower pulse energies, corresponding to the formation of smooth waveguides, laser pulses first melt the glass, producing a molten cylindrical volume, along the Z -writing direction, which then becomes denser during the solidification process. This corresponds to the regime of smooth waveguide formation. At higher energies we found that the instability with a well-defined threshold occurs. The origin of this instability is not yet completely clear.

As first possible mechanism, we consider threshold-like absorption [20, 22] triggered by a high temperature. Strong single-photon absorption occurs in glass at temperatures above 1500 K [22]. The fraction of absorbed energy then rapidly increases, and a hot (bright) spot is formed with $T \sim 5000$ K, which moves backwards along the laser beam [13, 23] in an auto-soliton manner. Dense, hot plasma forms in accordance with this model. The material dissociates (partially) inside this hot spot and consists of a gas and plasma mixture. Estimation of the internal pressure gives a level of a few GPa. This is a typical pressure level when various glasses become densified – up to a dozens of percents. To explain micro-void-like formation, the mechanism of charged layer formation on a liquid–plasma interface due to different particle mobilities was introduced in [20]. The effective surface tension could have a negative sign in accordance with this mechanism. This is essential, since any increase in surface area will be energetically profitable. When the upper, biggest pearls are formed, the absorption drops, the structure scatters light and strongly distorts the focus of the beam and partially explains the observed reduction in white light generation. In addition, the glass cannot be further modified by the laser pulses, probably due to the fact that the material is already dense.

A second possible explanation concerns the hydrodynamic instability. The effect leading to formation of pearl-

chain structures looks analogous to the breakup of a liquid jet in air, decaying spontaneously into drops. The liquid material, having an energetically unfavorable shape, contracts to a sphere by surface tension. The formation of drops in surface-tension-driven liquid flows was first explained by Rayleigh, who considered small periodic perturbations of a liquid cylinder with a radius r_0 . Rayleigh showed that at a certain perturbation wavelength, $\Lambda_R \approx 9r_0$, determining also the size of the drops, perturbations grow fastest [24]. The characteristic parameter for the jet decay is given by the reduced wave number $x = 2\pi r_0/\Lambda_R$. If $x < 1$, the jet is unstable and breaks into drops in a regular periodic fashion. For $x > 1$ irregular breakup is observed.

In our case, high laser powers produce a melted cylinder of liquid glass inside the bulk which is unstable and is assumed to decay spontaneously into drops. If we adopt the ‘hydrodynamic instability’ mechanism a qualitative picture of the processes involved in the laser fabrication of waveguide can be described as follows: first, the solid material is melted by a single or a sequence of laser pulses. Every subsequent laser pulse then results in the heating of the molten liquid. The solid–liquid interface velocity is determined by the temperature of the molten material and, immediately after the laser pulse, is first high and then slows down. This produces a modulation of the velocity of the molten liquid jet at the laser repetition rate. In this case one has $\Lambda = u/f$, where u is the velocity of the molten liquid jet, which is determined by the velocity of the liquid–solid interface, and f is the repetition rate of the laser system. For laser melting, typical liquid–solid interface velocities are of the order of 100 m/s [25]. Using this value and $f = 10$ MHz, we get for the perturbation wavelength $\Lambda = 10$ μm , which corresponds approximately to the period of the observed pearl-chain structures in the horizontal direction. The time scale on which jet perturbations grow is determined by $\tau = (\rho r_0^3/\gamma)^{1/2}$, where ρ is the density and γ is the coefficient of the surface tension of the liquid [11]. An estimate of this time can be obtained using data for molten glass [26]: $\rho \approx 2.8 \times 10^3$ (kg/m³), $\gamma \approx 0.1$ (N/m), and $r_0 \approx 1$ μm , which gives $\tau \approx 1.7 \times 10^{-7}$ s and is close to the temporal distance between laser pulses (10^{-7} s) defined by the repetition rate of our laser system. Viscosity and the surrounding solid material produce damping effects on the motion of the molten liquid caused by the surface tension. Therefore, the formation of regular droplets can be observed only at sufficiently high laser energies (melt temperatures) when the viscosity is reduced. Rapid cooling and solidification of the molten material produces the observed pearl-chain structures. There are several problems with the last model: the liquid cylinder is generated inside the solid glass matrix. Therefore, the size of the drops is limited by the surrounding solid material and cannot be much bigger than the initial cylinder radius. In this case (if the surface tension is positive) a cylinder shape is energetically more favorable than that of a set of drops with the same (or smaller) radius. One can avoid this complication assuming a negative surface tension again.

4.5 Refractive index contrast: comparison

Waveguide properties of pearl-chain structures have to be further investigated in terms of transmission and

optimization. Optical transmission is expected to be higher in the case of our smooth waveguides than in the case of pearl-chain waveguides. Losses in structures of this type cannot be comparable either to those in traditional telecom fibers with an index contrast of 5×10^{-3} and aperture 0.14. The numerical aperture of the pearl-chain waveguide is 0.18 (due to the high change of the refractive index $\sim 10^{-2}$, allowing simple beam coupling. Last but not least, bending losses in the case of pearl-chain waveguides can be much lower than those for smooth waveguides, allowing, in principle, the fabrication of bent structures.

In comparison, the maximum change in the refractive index for a smooth waveguide in fused silica at a low repetition rate is lower than 10^{-3} at the “optimum” pulse energy of 750 nJ [14], which is of the same order of magnitude as in our case (but with a pulse energy of ~ 30 nJ). The writing speed in [14] is $10 \mu\text{m/s}$, i.e., 100 times slower than in our case. Results in [7] obtained at a wavelength of 1045 nm with rather long laser pulses (375 fs) also show higher refractive index contrast at higher pulse repetition rates. In [6], using laser pulses of 115 nJ at 532 nm and a pulse duration of 500 fs, waveguides were fabricated with a writing speed of 0.05 mm/s. The refractive index contrast for smooth waveguides was estimated as 1×10^{-2} and the measured losses were below 1 dB/cm. In [6], the authors mention that for shorter writing wavelength optical losses become lower. Neither in [6] nor in [8] was the transverse micro-void structure seen during waveguide writing, whereas there are recent experimental papers where self-organized arrays of micro-voids were formed in the direction of the beam propagation [22, 23]. In our work, we have not yet investigated possibilities of optimizing waveguide losses using different focusing optics.

Recently, we found that waveguides which look similar to the pearl-chain ones under the microscope were formed in a point-by-point manner with the help of a low repetition-rate system [9, 27]. This also corresponds to what we have seen in separate experiments with a different laser system operating at a repetition rate of 1 kHz (Spitfire, Spectra-Physics), but this discussion would be beyond the scope of the present paper. Suffice it to mention here that the physics in the MHz and kHz cases are quite different.

5 Conclusions and visible perspectives of pearl-chain waveguides

The application of high energy 27 fs 26 nJ laser pulses at 10 MHz pulse repetition rate allowed us to demonstrate new type of pearl-chain waveguides. At energies below 26 nJ smooth waveguides have been written. Qualitative explanation of the origin of regular pearl-chain structures is given. Pearl-chain waveguides have higher refractive index contrast and can be used for the fabrication of cou-

plers and small-radius-bent structures. One could think of using a pearl-chain waveguide as a pre-form for a diameter-modulated channel. Such a channel (in shape of a capillary), being filled with the gas, already allowed the demonstration of dramatic, by a factor of 10^3 enhancement of the yield of high harmonics generated with intense fs pulses [28]. The pearl-chain writing technique developed in this work, in conjunction with etching technique, could in near future provide even a diameter-modulated channel with the properly chirped period for efficient quasi-phase matching in presence of propagation effects.

ACKNOWLEDGEMENTS We appreciate the interest of I. Bennion in this work and valuable discussions with A. Marcinkevicius, V. Mezentsev and E. Podivilov. We are indebted to M. Renke and A. Sugita for their help and to P. Kazansky and V. Astratov for their comments.

REFERENCES

- 1 E.N. Glezer, E. Mazur, *Appl. Phys. Lett.* **71**, 882 (1997)
- 2 C.B. Schaffer, A. Brodeur, J.F. Garcia, E. Mazur, *Opt. Lett.* **26**, 93 (2001)
- 3 C. Hnatovsky, R.S. Taylor, P.P. Rajeev, E. Simova, V.R. Bhardwaj, D.M. Rayner, P.B. Corkum, *Appl. Phys. Lett.* **87**, 014 104 (2005)
- 4 R. Osellame, N. Chiodo, G.D. Valle, S. Taccheo, R. Ramponi, G. Cerullo, A. Killi, U. Morgner, M. Lederer, D. Kopf, *Opt. Lett.* **29**, 1900 (2004)
- 5 R. Osellame, S. Taccheo, M. Marangoni, R. Ramponi, P. Laporta, D. Polli, S. De Silvestri, G. Cerullo, *J. Opt. Soc. Am. B* **20**, 1559 (2003)
- 6 L. Shah, A.Y. Arai, S.M. Eaton, P.R. Herman, *Opt. Express* **13**, 1999 (2005)
- 7 S.M. Eaton, H. Zhang, P.R. Herman, F. Yoshino, L. Shah, J. Bovatsek, A.Y. Aral, *Opt. Express* **13**, 4708 (2005)
- 8 L. Tong, R.R. Gattass, I. Maxwell, J.B. Ashcom, E. Mazur, *Opt. Commun.* **259**, 626 (2006)
- 9 X.H. Zhang, S.M. Eaton, P.R. Herman, *Opt. Express* **14**, 4826 (2006)
- 10 A. Fernandez, T. Fuji, A. Poppe, A. Fürbach, F. Krausz, A. Apolonski, *Opt. Lett.* **29**, 1366 (2004)
- 11 M.R. Teague, *J. Opt. Soc. Am. B* **72**, 1199 (1982)
- 12 M.R. Teague, *J. Opt. Soc. Am. B* **73**, 1434 (1983)
- 13 S. Kanehira, J. Si, J. Qiu, K. Fujita, K. Hirao, *Nano Lett.* **5**, 1591 (2005)
- 14 A. Streltsov, N.F. Borrelli, *J. Opt. Soc. Am. B* **19**, 2496 (2002)
- 15 A. Brodeur, S.L. Chin, *J. Opt. Soc. Am. B* **16**, 637 (1999)
- 16 A. Gaeta, *Phys. Rev. Lett.* **84**, 3582 (2000)
- 17 P.B. Corkum, P.P. Ho, R.R. Alfano, J.T. Manassah, *Opt. Lett.* **10**, 624 (1985)
- 18 I.A. Bufetov, E.M. Dianov, *Physics Uspekhi* **175**, 91 (2005) (English edition of *Uspekhi Fizicheskikh Nauk*)
- 19 R.M. Atkins, P.G. Simpkins, A.D. Yablon, *Opt. Lett.* **28**, 974 (2003) and references therein
- 20 S.I. Yakovlenko, *Quantum Electron.* **34**, 765 (2004)
- 21 S.I. Yakovlenko, *Laser Phys.* **16**, 474 (2006)
- 22 S.I. Yakovlenko, *Quantum Electron.* **34**, 787 (2004)
- 23 E. Toratani, M. Kamata, M. Obara, *Microelectron. Eng.* **83**, 1782 (2006)
- 24 J. Eggers, *Rev. Mod. Phys.* **69**, 865 (1997)
- 25 D. Bäuerle, *Laser Processing and Chemistry* (Springer, Berlin, Heidelberg, 2000) p. 171
- 26 E. Guyon, J.-P. Hulin, L. Petit, C.D. Matescu, *Physical Hydrodynamics* (Oxford University Press, New York, 2001), p. 55
- 27 E. Toratani, M. Kamata, M. Obara, *Appl. Phys. Lett.* **87**, 171 103 (2005)
- 28 A. Rundquist, C.G. Durfee III, Z. Chang, C. Herne, S. Backus, M.M. Murnane, H.C. Kapteyn, *Science* **280**, 1412 (1998)